Origin, trafficking, and intraepithelial fate of gut-tropic T cells

Delphine Guy-Grand,[1,6] Pierre Vassalli,[7] Gerard Eberl,[2,8] Pablo Pereira,[1,6] Odile Burlen-Defranoux,[1,6] Fabrice Lemaitre,[3,6] James P. Di Santo,[4,6] Antonio A. Freitas,[5,8] Ana Cumano,[1,6] and Antonio Bandeira[5,8]

[1]Unité de Lymphopoièse, [2]Unité de Developpement des Tissus Lymphoïdes, [3]Unité de Dynamiques des Réponses Immunes, [4]Unité d'Immunité Innée, [5]Unité de Biologie des Populations Lymphocytaires, Institut Pasteur, 75015 Paris, France
[6]Institut National de la Santé et de la Recherche Médicale, Unité 668, 75015 Paris, France
[7]Departement de Pathologie, Centre Médical Universitaire, CH-1211, Genève, Switzerland
[8]Centre National de la Recherche Scientifique, URA 1961, 75015 Paris, France

The small intestine epithelium (SI-Ep) harbors millions of unconventional (γδ and CD4$^-$ CD8$^-$ NK1.1$^-$ TCRαβ) and conventional (CD8αβ and CD4) T cells, designated intraepithelial lymphocytes (IELs). Here, we identified the circulating pool of SI-Ep–tropic T cells and studied their capacity to colonize the SI-Ep under steady-state conditions in SPF mice. Developmentally regulated levels of α4β7 endowed recent thymic emigrants (RTEs) of unconventional types with higher SI-Ep tropism than their conventional homologues. SI-Ep–tropic RTEs, which in all lineages emerged naive, homed to the SI-Ep, but this environment was inadequate to stimulate them to cycle. In contrast, conventional and, unexpectedly, unconventional T cells, particularly Vγ7$^+$ (hallmark of γδ IELs), previously stimulated to cycle in the gut-associated lymphoid tissue (GALT), proliferated in the SI-Ep. Cycling unconventional SI-Ep immigrants divided far more efficiently than their conventional homologues, thereby becoming predominant. This difference impacted on acquisition of high Granzyme B content, which required extensive proliferation. In conclusion, SI-Ep–tropic T cells follow a thymus–SI-Ep or a GALT–SI-Ep pathway, the latter generating highly competitive immigrants that are the sole precursors of cytotoxic IELs. These events occur continuously as part of the normal IEL dynamics.

CORRESPONDENCE
Delphine Guy-Grand:
guygrand@pasteur.fr
OR
Antonio Bandeira:
antonio.bandeira-ferreira@pasteur.fr

Abbreviations used: GALT, gut-associated-lymphoid-tissue; IEL, intraepithelial lymphocyte; LP, lamina propria; LPL, LP lymphocyte; MLN, mesenteric LN; PLN, peripheral LN; PP, Peyer's patches; RTE, recent thymic emigrant; SI-Ep, small intestinal epithelium; SI-LP, small intestinal lamina propria; TDL, thoracic duct lymphocyte; uncTCRαβ cells, unconventional TCRαβ cells

In mice, villi of the small intestinal epithelium (SI-Ep) harbors ∼50 millions T cells, named intraepithelial lymphocytes (IELs), representing up to half the number of T cells in the organism (Rocha et al., 1991). IELs are composed of conventional TCRαβ cells expressing the CD4 or the heterodimer CD8αβ co-receptors, and unconventional (unc) TCRαβ cells (so-called CD8αα, type b or natural IELs) and TCRγδ cells lacking CD4/CD8αβ co-receptors (Cheroutre et al., 2011). Many IELs are highly cytotoxic (Goodman and Lefrancois, 1989; Guy-Grand et al., 1996; Müller et al., 2000), and are characterized morphologically by cytoplasmic granules with high Granzyme B content (Guy-Grand et al., 1991). Full IEL development requires microbe-promoted stimulations (Guy-Grand et al., 1978; Bandeira et al., 1990).

In normal euthymic mice, IEL precursors are of thymic origin (Guy-Grand et al., 2003; Cheroutre et al., 2011). Migration to the SI depends on the integrin α4β7 (Wagner et al., 1996; Lefrançois et al., 1999) whose ligand MadCAM-1 is expressed by the venules of the lamina propria (LP; Berlin et al., 1993). CCR9 and its ligand, CCL25, expressed by the SI-Ep, play an additional role (Zabel et al., 1999), but inactivation of one of these molecules only results in a marked deficit of γδ IELs (Wurbel et al., 2001, 2007). α4β7 and CCR9 are designated "gut-tropic" molecules.

For conventional T cells, acquisition of gut-tropic molecules appears to be largely restricted to cells activated in the gut-associated lymphoid tissue (GALT), which is composed of Peyer's patches (PPs), mesenteric lymph nodes (MLN), and isolated lymphoid follicles from the LP (Guy-Grand et al., 1978; Mora et al., 2003; Cheroutre et al., 2011; Cauley and Lefrançois,

The Rockefeller University Press $30.00
J. Exp. Med. 2013 Vol. 210 No. 9 1839-1854
www.jem.org/cgi/doi/10.1084/jem.20122588

The Journal of Experimental Medicine

2013). At these sites, up-regulation of gut-tropic molecules requires stimulation by retinoic acid-synthesizing CD103$^+$ DC (Iwata et al., 2004; Stock et al., 2013). Activated T cells then migrate to the thoracic duct as cycling blasts, and reach the SI-Ep via the blood stream (Guy-Grand et al., 1978; Guy-Grand and Vassalli, 1986). The view that naive cells do not home to the SI-Ep was challenged by evidence that CD8αβ recent thymic emigrants (RTEs) efficiently seed the SI-Ep (Staton et al., 2006), but their contribution to the respective IELs has not been clearly assessed.

In contrast, rules governing migration of TCRγδ and uncTCRαβ T cells to the SI-Ep are poorly defined. The notion is that acquisition of gut-tropic molecules also requires activation but in the context of their development in the thymus (Lafaille et al., 1989; Gangadharan et al., 2006; Vantourout and Hayday 2013), although some gut-tropic γδ T cells exit the thymus in a naive state (Jensen et al., 2009). Only cells bearing particular TCRγ families, i.e., TCR Vγ7$^+$ cells (nomenclature of Heilig and Tonegawa, 1986), are programmed to "directly" home to the SI-Ep, without prior traffic through the GALT (Cheroutre et al., 2011), but such pathway has never been fully characterized.

Under steady-state conditions, the contribution of circulating cells to the dynamics of IELs appears rather limited, as the SI-Ep is considered of restricted accessibility (Poussier et al., 1992), because of the long life span of resident IELs. This view is difficult to reconcile with the continuous development of conventional T cell–mediated natural immune responses in the GALT, or with the continuous thymic output of newly generated, gut-tropic unconventional T cells.

To understand the general rules of homing and colonization of the SI-Ep in physiological conditions, we studied the origin, traffic pattern, population dynamics, and differentiation of T cells continuously seeding the SI-Ep in normal adult SPF mice.

RESULTS

Quantitative differences between T cells in the SI-Ep and in the hemolymphatic circuit

In the SI-Ep, T cell populations are characterized by the predominance of cells of the unconventional type (Table 1), ∼50% being γδ cells and 20% (CD8β$^-$ CD4$^-$ NK1.1$^-$) uncTCRαβ cells, and by a CD4/CD8αβ T cell ratio of 0.5. Lymph, from the thoracic duct (Table 1), and blood (not depicted) contained mainly CD4$^+$ and CD8αβ T cells, at a ratio of 1.6, and very few γδ (1.4%) and uncTCRαβ (0.6%) cells.

The highest differential between the two compartments was the frequency of Vγ7$^+$ cells: ∼30% in IELs versus ∼0.1% in thoracic duct lymphocytes (TDLs). As the number of T cells recovered from the thoracic duct after 18 h drainage is close to that of IELs (∼40 versus ∼50 millions), the pool size of Vγ7$^+$ cells, circulating during that period, is ∼300-fold smaller than that of the respective IEL population. This result underlines the issue of the competitiveness of rare circulating cells in effectively seeding the SI-Ep, whose niches are occupied by large numbers of resident cells.

To identify cells in circulation that might continuously colonize the SI-Ep, we studied the expression of gut-tropic molecules in TDLs according to their age and activation status.

Thymic development confers higher gut tropism to γδ and uncTCRαβ T cells than to their conventional homologues

Using RAG2p-GFP transgenic mice, we determined the expression levels of α4β7 and CCR9 in newly generated T cells at the stage of RTEs, identified by the expression of GFP, which persists for ∼3 wk after down-regulation of RAG-2 gene transcription (Guy-Grand et al., 2003; Boursalian et al., 2004).

In the lymph of 6-wk-old mice, TDLs contained a high frequency of GFP$^+$ cells (Fig. 1 A), hereafter referred to as RTEs, which in all T cell types were CD62L^{high} CD44$^{low/int}$, i.e., naive (not depicted). The proportion of γδ T cells was higher than in global TDLs (Table 1) Unconventional RTEs expressed 3.4–6-fold higher levels of α4β7 than their conventional homologues (Fig. 1 A). γδ RTEs expressed the highest levels of CCR9, which was undetectable in CD4$^+$ RTEs and in most uncTCRαβ RTEs (Fig. 1 A).

The differential expression of gut-tropic molecules among lineages was developmentally related, as it was already apparent (albeit less markedly so) among the respective newly generated mature thymocytes (Fig. 2), defined as TCR^{high} CD69$^-$ GFP$^+$, which in all lineages were CD44$^{low/int}$. In contrast, TCR^{high} CD69$^-$ GFP$^-$ thymocytes in all lineages

Table 1. T-cell subset distribution in IELs and TDLs

	Frequency				
CD3$^+$	γδ	Vγ7	uncTCRαβ[c]	CD8αβ	CD4
	%	%	%	%	%
IELs[a]	46.5 ± 11.5 (49)	30.6, 65.9 ± 9.6 (8)[d]	20.08 ± 7.4 (47)	21.2 ± 9.7 (47)	10.3 ± 6 (47)
TDLs[a]	1.44 ± 0.5 (52)	0.08, 5.6 ± 2.2 (14)[d]	0.59 ± 0.3 (39)	37.7 ± 6.8 (40)	58.9 ± 7.1 (40)
RTEs[b]	2.65 ± 1 (8)	0.24, 11.5 ± 1.4 (3)[d]	0.71 ± 0.4 (9)	24 ± 3.8 (8)	72.1 ± 4.4 (8)

Values in parentheses show the number of mice individually analyzed.
[a]Percent CD3$^+$ cells: TDLs, 76 ±10; IELs, 84 ± 6.9.
[b]6–12 wk-old RAG2p-GFP mice. Percent GFP$^+$ in CD3$^+$ TDLs: 23 ± 2.6. The frequency of unconventional T cells in RTEs was independent of the age of the mice.
[c]NK-T cells were excluded with an anti-NK1.1 mAb. Similar results were obtained in CD1$^{-/-}$ mice.
[d]Percent Vγ7$^+$ in γδ T-cells.

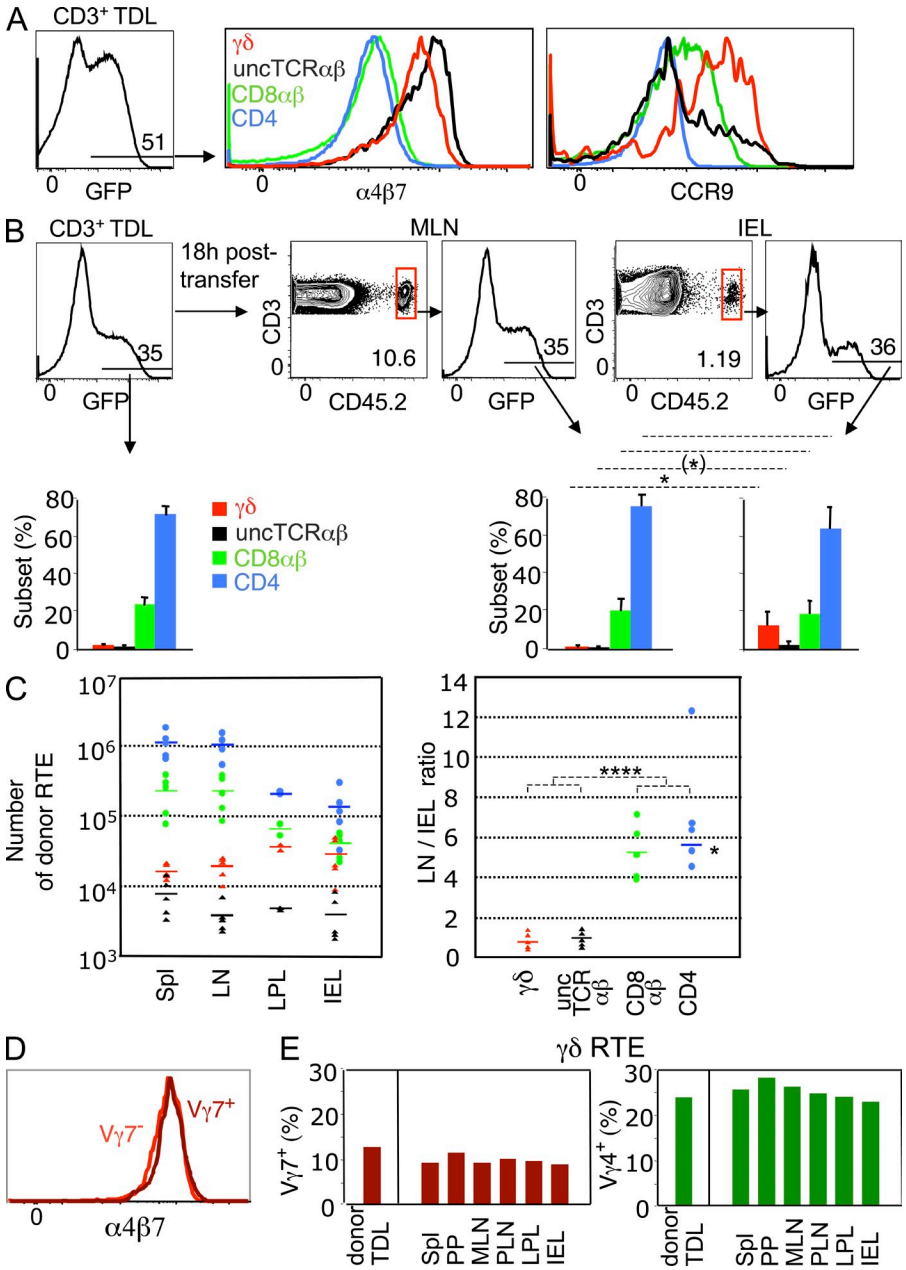

Figure 1. SI-Ep tropism of RTEs. (A) RTEs from 6-wk-old RAG2p-GFP (CD45.2) B6 mice were assessed for expression of gut-tropic molecules by flow cytometry. (left) Frequency of GFP+ (RTEs) cells in CD3+ TDLs. (right) Expression of α4β7 and CCR9 in the indicated T cell subsets of GFP+ cells. α4β7 mean fluorescence intensity (MFI): 5602 (γδ), 7750 (uncTCR αβ), 1624 (CD8αβ), 1296 (CD4). CCR9 MFI: 3412 (γδ), 1865 (uncTCR αβ), 1151 (CD8αβ), 493 (CD4). Data correspond to six mice, individually studied in five independent experiments (α4β7), and to three mice, in three independent experiments (CCR9). (B) RAG2p-GFP TDLs were transferred to wild-type (CD45.1) B6 recipients and analyzed 18 h later. Dot plots show the frequency of donor CD3+ TDLs in MLN and SI-Ep. Histograms show the frequency of GFP+ cells and respective T cell subset distribution (bar graphs) in donor TDLs (eight mice individually studied in seven independent canulation experiments) and in the indicated recipient's organs (five mice in five independent transfer experiments). *, $P < 0.02$; (*), $P = 0.056$. (C, left) Absolute number of donor RTEs in the indicated organs of the recipients described in B. Values are based on the total number of CD3+ cells per organ, calculated as described in Materials and methods. Arithmetic means are indicated. (C, right) Ratio of the number of donor cells in LN versus SI-Ep for each T cell subset. For CD4 T cells, the average ratio (see asterisk) did not take into account the outlier value. ****, $P < 0.0001$ (pooled unconventional versus conventional LN/IEL ratios). (D) Expression of α4β7 in Vγ7+ and Vγ7− GFP+ (RTEs) TDLs (two mice studied in two independent experiments). (E) RAG2p-GFP TDLs were transferred to wild-type (CD45.1) B6 recipients and analyzed 18 h later. The histograms show the frequency of Vγ7+ and Vγ4+ cells in GFP+ (RTEs) cells in the indicated organs. A second recipient, in another transfer experiment, gave similar results: the average frequency, as percentage of γδ RTEs, of all pooled organs was as follows: Vγ7+, 11.2 ± 2.5; Vγ4+, 23.2 ± 4.1. In detail, for IELs 13.7% (Vγ7+) and 23.9% (Vγ4+), for MLN 9.8% (Vγ7+) and 20.4% (Vγ4+), for the spleen 10.2% (Vγ7+) and 20.3% (Vγ4+).

were in majority CD44^{high} and expressed neither α4β7 nor CCR9 (Fig. 2). Thus, the contribution of the thymus to the circulating pool of gut-tropic T cells appears restricted to cells with a naive phenotype, whose levels of α4β7 are highest at the stage of RTE.

To assess whether levels of α4β7 and CCR9 in RTE correlated with SI-Ep homing efficiency, TDLs of RAG2p-GFP B6 mice (CD45.2) were transferred to nonirradiated B6-CD45.1 recipients. At 18 h after transfer, the frequency of donor cells, as percentage of host CD3+ cells, was considerably lower in the SI-Ep (1.2%) and the SI-LP (3%), than in MLN, peripheral LN (PLN), and spleen (10–12%; Fig. 1 B and not depicted). At all these sites, RTEs (GFP+) were at a frequency as high as in the transferred TDL cohort (Fig. 1 B), but the T cell lineage composition was sharply distinct in the SI-Ep: whereas unconventional cells accounted for ≤3% in LN or spleen, and ∼5% in the SI-LP, they represented up to 20% of RTEs in the SI-Ep, corresponding to an enrichment

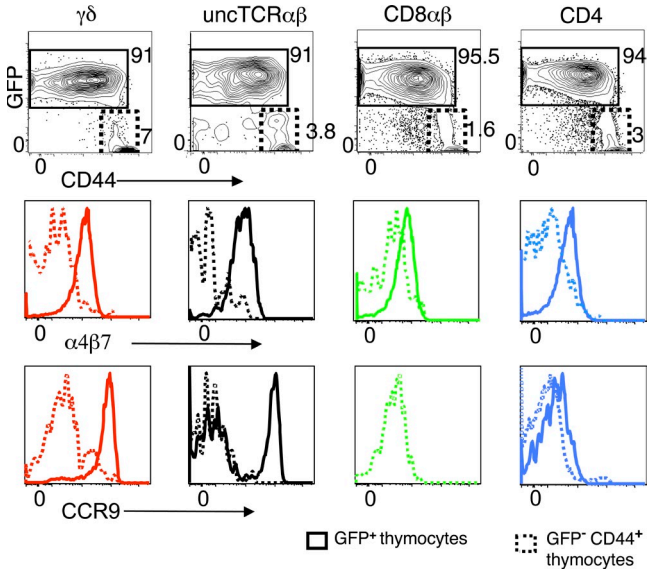

Figure 2. Expression of α4β7 and CCR9 in newly generated mature thymocytes. Thymocytes of a RAG2p-GFP mouse were gated on CD69$^-$ TCR^{high} cells. Gates delineate GFP$^+$ CD44$^{low/int}$ and GFP$^-$ CD44^{high} subsets in the indicated populations. Histograms show an overlay of α4β7 or CCR9 profiles in GFP$^+$ versus GFP$^-$ subsets for each T cell lineage. α4β7 MFI of GFP$^+$ versus GFP$^-$ subsets: 1273 versus 238 (γδ), 926 versus 50 (uncTCR αβ), 616 versus 285 (CD8αβ), and 524 versus 173 (CD4). CCR9 MFI of GFP$^+$ versus GFP$^-$ subsets: 7400 versus 859 (γδ), 3732 versus 119 (uncTCR αβ), 776 versus 318 (CD8αβ), and 318 versus 252 (CD4). For comparison, the MFI of DP thymocytes were 250 for α4β7, and 2019 for CCR9. Profiles are representative of four mice individually studied in three independent experiments.

of 6–10-fold for γδ cells, and 3–5-fold for uncTCRαβ cells (Fig. 1 B and not depicted).

In conclusion, the SI-Ep is continuously open to all types of RTEs, but access to this site is biased toward T cells of the unconventional type, in line with the higher levels of gut-tropic molecules expressed by these cells.

γδ and uncTCRαβ RTEs home to the SI-Ep and secondary lymphoid organs with similar efficiency

Like their conventional homologues, unconventional RTEs expressed CD62L (unpublished data). To better define the pattern of recirculation of these cells endowed with both high SI-Ep and LN homing capacity, we estimated the absolute number of RTEs per organ.

As shown in Fig. 1 C, the number of conventional RTEs in total LN (or spleen) was considerably higher than in the SI-Ep (or SI-LP; left), with an average LN/SI-Ep ratio of five to six for CD8αβ$^+$ or CD4$^+$ T cells (right). In contrast, the number of unconventional RTEs was of the same order at all sites, with an average LN/SI-Ep ratio of ∼1 for γδ or uncTCRαβ RTEs (Fig. 1 C).

In conclusion, unconventional RTEs have a similar probability of entering the intestinal wall or secondary lymphoid organs, whereas conventional RTEs circulate preferentially through secondary lymphoid organs.

SI-Ep tropism is a general property of γδ RTEs

The fact that the overwhelming majority of newly generated γδ T cells expressed gut-tropic molecules suggested that the paradigm that cells bearing particular TCRγ families are programmed in the thymus to home to specific peripheral sites might not apply to the SI-Ep.

In the thymus, the expression of gut-tropic molecules in cells expressing Vγ7, which is the dominant TCRγ family in IELs, was almost exclusively confined to GFP$^+$ cells, which were CD62L^{high} CD44^{low} (unpublished data). Vγ7$^+$ cells represented 12% of γδ RTE TDLs (Table 1), and their α4β7 or CCR9 expression profiles were perfectly superimposable on those of Vγ7$^-$ RTEs (Fig. 1 D and not depicted). This suggested that RTEs expressing Vγ families poorly represented in the SI-Ep, i.e., Vγ4 (25–30% in circulating γδ RTEs versus <10% in γδ IELs), should have a SI-Ep homing potential equivalent to that of Vγ7$^+$ RTEs. Indeed, at 18 h after transfer, the frequency of both γδ subsets in all organs was similar to that in transferred TDLs, Vγ4$^+$ cells outnumbering Vγ7$^+$ cells in the SI-Ep, as at all other sites (Fig. 1 E).

In conclusion, SI-Ep tropism is a general property of newly generated γδ T cells in the adult, implying that the predominance of Vγ7$^+$ cells in IELs is not developmentally determined.

TDLs with the highest levels of α4β7 and CCR9 are GALT-related conventional and unconventional cycling blasts, highly enriched in Vγ7$^+$ cells

Next, we assessed the expression of gut-tropic molecules in TDLs defined according to the activation status. In each TDL T cell subset, a minor fraction of cells expressed 10–20-fold higher levels of α4β7 and CCR9 than the respective GFP$^+$ RTEs (Fig. 3 A), but low levels of CD62L (not depicted). These cells were CD44^{high} (Fig. 3 A), large sized (not depicted), and expressed high levels of the cell cycle marker Ki-67 (Fig. 3 B). The presence in the thoracic duct lymph of conventional cells with these properties was expected, as they correspond to the classical description of circulating cycling blasts generated upon immune responses in the GALT (Cheroutre et al., 2011). The unexpected finding here was the identification of cycling blasts of the unconventional type (Fig. 3, A and B), highly enriched in α4β7^{high} CCR9^{high} CD44^{high} TDLs, as compared with total TDLs (Fig. 3 C). Remarkably, Vγ7$^+$ cells accounted for ∼50% of α4β7^{high} Ki-67^{high} γδ TDLs, against 6% in naive γδ TDLs (Fig. 3 D). Of note, whereas most CD44^{high} γδ TDLs had lost α4β7, most corresponding Vγ7$^+$ TDLs had up-regulated this molecule (Fig. 3 A, blue gates), indicating that they were preferentially activated under conditions that reinforce gut tropism.

We then searched for cells with similar features in lymphoid structures drained by the thoracic duct. Both conventional and unconventional α4β7^{high}CD44^{high} blasts, highly enriched in Vγ7$^+$ cells, were found in MLN but not in PLN (Fig. 3 E), indicating that the GALT was the source of those blasts. In MLN, a fraction of conventional and uncTCRαβ α4β7^{high}CD44^{high} blasts expressed CD69 (not depicted), a molecule attesting activation but also retention in the tissue,

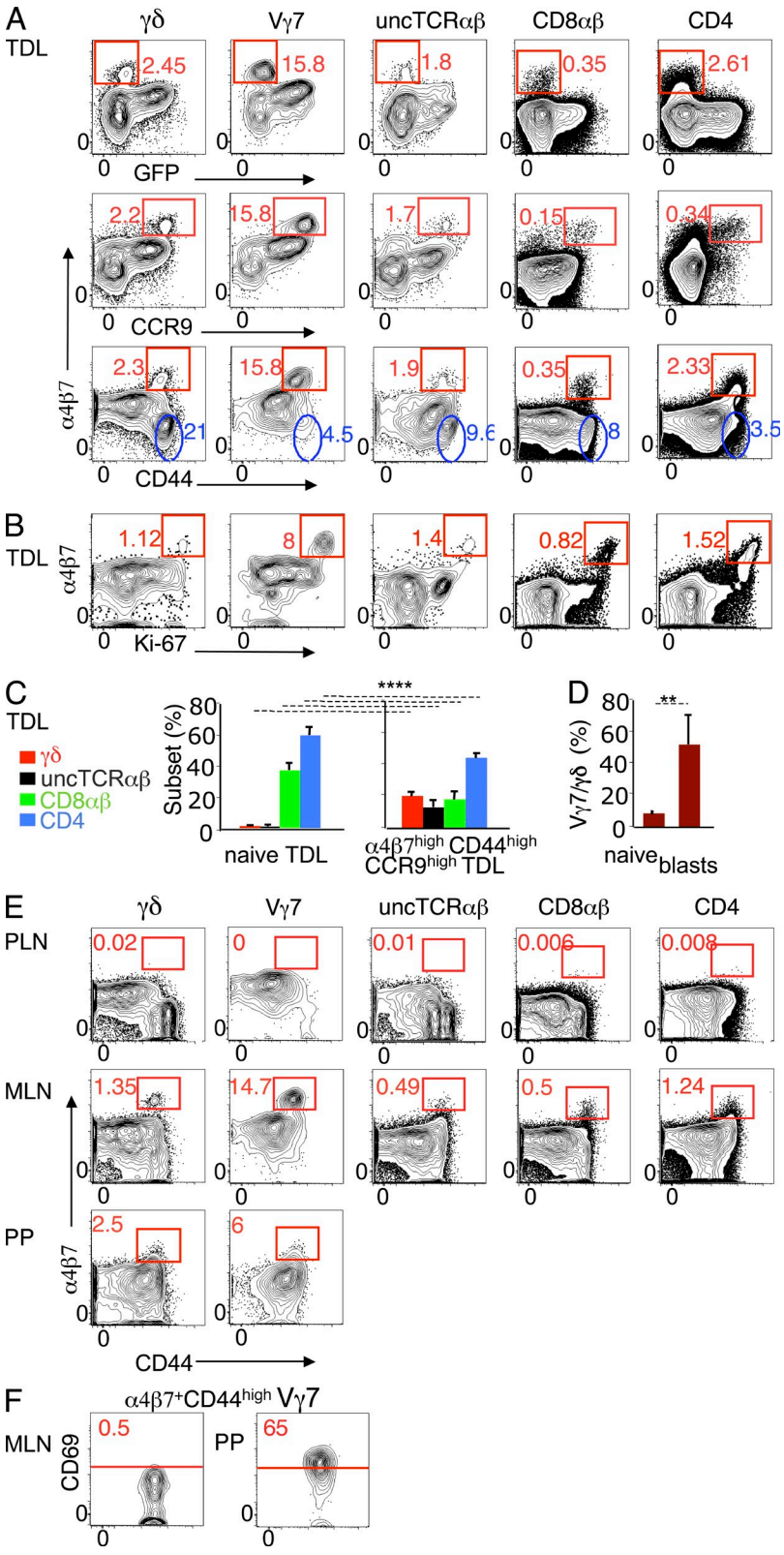

Figure 3. Conventional and unconventional cycling TDL blasts express the highest levels of gut-tropic molecules and are GALT-related. TDLs of 8–12-wk-old RAG2p-GFP mice were assessed for expression of gut-tropic molecules by flow cytometry. (A) Dot plots show α4β7 versus GFP, CCR9, or CD44 (eight mice individually studied in seven independent experiments). Red gates define cells expressing high levels of α4β7 lacking GFP or coexpressing high levels of CD44 or CCR9. α4β7 MFI in α4β7^{high} GFP^{-} (CD44^{high}) versus GFP^{+} (CD44^{low}) TDLs: γδ, 15133/1758; Vγ7, 15139/1833; uncTCRαβ, 15321/780; CD8αβ, 7427/369; CD4, 5113/397. Blue gates indicate CD44^{high} TDLs that lack α4β7. (B) Dot plots showing α4β7 versus Ki-67 expression (three mice in three independent experiments). (C) T cell subset distribution in naive (CD44^{low}) and α4β7^{high} CCR9^{high} CD44^{high} TDLs from the mice described in A. ****, $P < 0.0001$. (D) Frequency of Vγ7^{+} cells in naive (CD44^{low}) and α4β7^{high} CCR9^{high} γδ TDLs (four mice in four independent experiments). **, $P < 0.003$. (E) Dot plots showing CD44 versus α4β7 expression in MLN, PLN (pool of brachial, axillary and inguinal LN) and PPs. MLN and PPs data are representative of 6 independent experiments, each with a pool of 2–3 mice. Two of these experiments included PLN, which in each case were a pool from 3 mice. (F) CD69 expression of α4β7^{high} CD44^{high} Vγ7^{+} cells in MLN and PPs, as gated in the corresponding panels in E.

since it counteracts S1PR1 required for exit to efferent lymphatics (Shiow et al., 2006; Bankovich et al., 2010). In contrast, corresponding γδ blasts, in particular Vγ7^{+}, lacked CD69 (Fig. 3 F). This "mobile" mode suggested that they might have been generated upstream. PPs, whose efferent lymphatics converge to MLN, contained α4β7^{+} CD44^{high} γδ blasts, in

particular Vγ7+ (Fig. 3 E), most of which expressed CD69 (Fig. 3 F). Thus, PPs might be one site where cycling γδ blasts are generated, but further dynamic studies are required to prove this point.

In conclusion, as in conventional T cells, recirculation through the GALT leads to selective priming of unconventional T cell subsets that reinforced SI-Ep tropism and diminished recirculation potential through LN.

Cycling TDL blasts home selectively to the SI-Ep, but they constitute a minor fraction of the immigrant population

Our results indicate that the pool of gut-tropic TDLs is essentially composed of naive cells and of few GALT-related cycling blasts, both enriched in unconventional cells. To assess whether these are the circulating cells that might continuously enter the SI-Ep, we analyzed the phenotype of TDL-derived immigrants in recipients sacrificed 18 h after transfer.

Donor SI-Ep immigrants were ∼0.5% of CD3+ IELs (∼10% in LN, spleen or blood), and the bulk of them lack CD69 (not depicted). They contained a high proportion of unconventional cells (Fig. 4 A) compared to donor TDLs (Table 1). In each T cell subset, ∼90% of the immigrants were CD44low/int (Fig. 4 B). CD44high CD3+ immigrants were Ki-67high and large sized (Fig. 4 C and not depicted). The resemblance of these cells with α4β7high CCR9high cycling TDLs was further documented by the similar T cell subset distribution, and the high frequency of Vγ7+ cells (Fig. 4 B; compare with Fig. 3, C and D).

Donor CD44high Ki-67high blasts were <1% of the immigrants in MLN and virtually undetectable in PLN (unpublished data), in line with their low levels of CD62L. They were also undetectable in the recipient's lymph collected between 24 and 44 h after transfer (not depicted). Together, these results suggest that most GALT-related blasts circulate for a short period before being selectively arrested in the SI wall.

In conclusion, the pool of SI-Ep immigrants resembles the set of cells in circulation previously identified on the basis of expression levels of gut-tropic molecules.

SI-Ep homing is highly dependent on α4β7

Levels of α4β7 were significantly lower in cycling SI-Ep immigrants than in the corresponding cells in circulation. This is compatible with down-regulation upon interaction with MadCAM, expressed by the venules of the SI-LP. The implication of this integrin in homing to the SI wall was confirmed by the strong reduction (85%) of the number of donor T cells in IELs (Fig. 4 C) and LP lymphocytes (LPLs; not depicted) in recipients under continuous treatment with a nondepleting anti-α4β7 mAb (Hamann et al., 1994; Staton

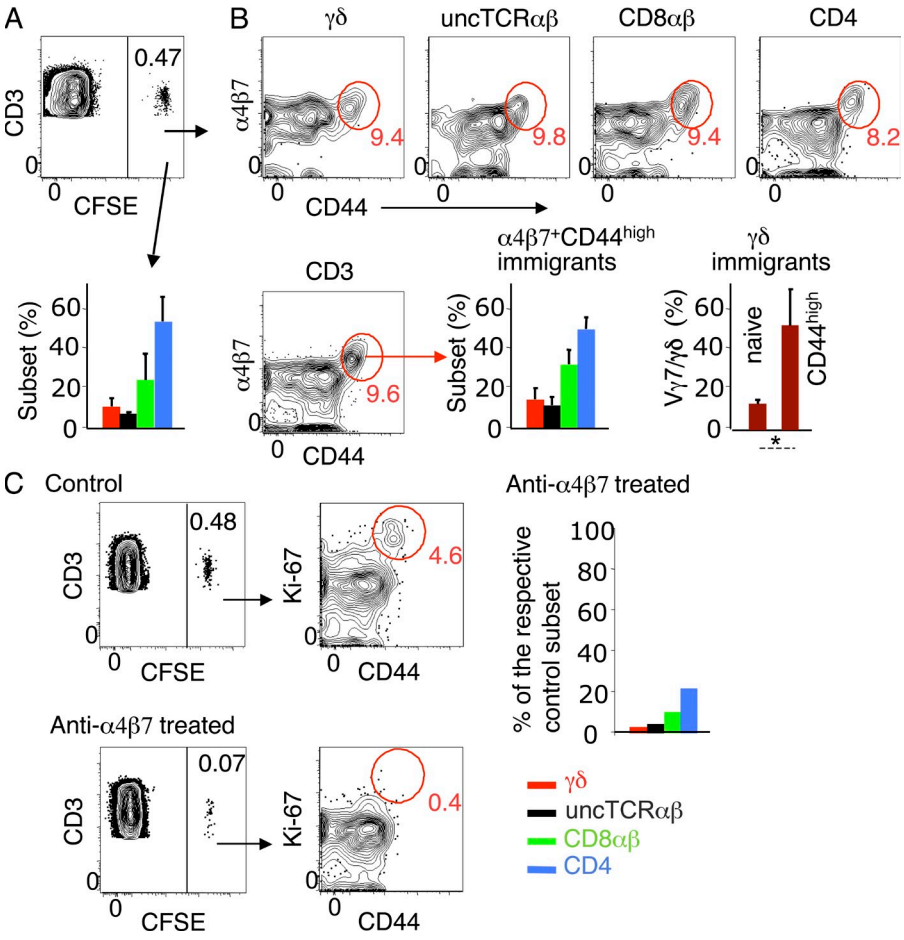

Figure 4. T cell subset distribution and phenotype of TDL-derived SI-Ep immigrants. CFSE-labeled CD45.2 B6 TDLs were transferred to wild-type CD45.1 B6 recipients, which were analyzed 18 h later. (A) Frequency of donor SI-Ep immigrants (mean ± SD: 0.48 ± 0.22; 8 recipients in 8 independent canulation and transfer experiments). Bar graph shows the corresponding T cell subset distribution (mean ± SD: γδ, 10.6 ± 3.6; uncTCRαβ, 6.8 ± 0.2; CD8αβ, 23.8 ± 12; CD4, 52.6 ± 11.5. (B, top) Frequency of α4β7+ CD44high cells in each T cell subset (mean ± SD: γδ, 9.8 ± 5.2; uncTCRαβ, 7.6 ± 7.1; CD8αβ, 8.2 ± 6.8; CD4, 7.4 ± 5.7) of the mice described in A. (B, bottom) Frequency of α4β7+ CD44high CD3+ immigrants (mean ± SD: 8.7 ± 3.7). (left) Respective subset distribution (mean ± SD: γδ, 11.0 ± 5.7; uncTCRαβ, 11.1 ± 7.0; CD8αβ, 29.0 ± 12.3; CD4, 49.3 ± 11.1). (right) Frequency of Vγ7+ cells in naive (CD44low) and CD44high γδ immigrants (three recipients in three independent experiments). *, P < 0.02. (C) Dot plots show the frequency and phenotype of donor SI-Ep immigrants in anti-α4β7–treated recipients (two treated recipients in two independent canulation and transfer experiments), and respective controls. Bar graph shows the number of immigrants in treated recipients, related to the number of the respective subset in untreated controls. Similar results were obtained in three treated recipients (each studied in an independent experiment) sacrificed 44 h after transfer.

et al., 2006). CD44^{high} Ki-67^{high} cells were hardly detectable (Fig. 4 C), and the number of unconventional and conventional naive immigrants was 3–5% and 10–20% of the corresponding subsets in untreated controls (Fig. 4 C). In contrast, the frequency of donor cells in spleen, MLNs, and PLNs was not significantly changed (unpublished data), in agreement with previous studies. Similar results were obtained in treated recipients sacrificed 44 h after transfer (unpublished data).

These results confirm, and extend to all T cell types, the major role of $\alpha4\beta7$ in SI-Ep homing, although some conventional naive cells might home in a $\alpha4\beta7$-independent manner.

RTEs arrested in the SI-Ep do not proliferate in situ

To study the potential of RTEs to colonize the SI-Ep, we assessed their capacity to react to local cues and to proliferate in situ. In a preliminary experiment, sorted GFP$^+$ (RTEs) TDLs of RAG2p-GFP mice were labeled with violet cell division tracer and transferred to nonirradiated animals. A control group received GFP$^-$ TDLs. At day 4 after transfer, no decay of the Violet tracer was observed in SI-Ep immigrants of recipients of GFP$^+$ TDLs, whereas significant decay was observed in the control group (unpublished data). In LN, few GFP$^+$ TDLs had proliferated, and decay of the violet tracer, indicative of up to five rounds of division, correlated with decay of GFP, which was still detected in most cells in the 3^d generation (unpublished data). The failure of RTEs to proliferate in the SI-Ep could not be explained by the lack of reactivity to local cues, as 40–50% of $\gamma\delta$ RTEs, including V$\gamma7^+$, had up-regulated CD69, as compared with 6–7% of CD4 and CD8$\alpha\beta$ RTEs (unpublished data).

Because RTEs that went through at least 3 rounds of division in LN could still be identified by the GFP, to obtain better yields of transferred RTEs, we repeated the aforementioned experiment with total TDLs. In general agreement with previous transfers, <3% of the RTEs in the SI-Ep had divided, and essentially only once, as compared with other immigrants that in 4 d generated progenies accounting for close to 40% of the GFP$^-$ SI-Ep donor population (Fig. 5 A). As also shown, many undivided unconventional RTEs, in particular V$\gamma7^+$, had up-regulated CD69, as compared with a minor fraction of conventional RTEs. The higher reactivity of unconventional RTEs to local signals was confirmed by the average frequency of CD69$^+$ RTEs at an earlier time point (44 h after transfer): ~20% in $\gamma\delta^+$, 30–40% in V$\gamma7^+$, and ~13% in uncTCR$\alpha\beta$, as compared with ~3% in CD8$^+$ and ~5% in CD4$^+$ RTEs (unpublished data).

We conclude that RTEs reacting to signals in the SI-Ep environment do not acquire competence to expand. Moreover, unconventional RTEs, in particular V$\gamma7^+$, are preferentially retained, whereas the overwhelming majority of conventional RTEs remain mobile.

Unconventional cycling SI-Ep immigrants have a higher proliferation potential than conventional homologues

To assess whether immigrants that proliferated extensively in the SI-Ep were progenies of cycling TDLs, a kinetic analysis of the proliferation pattern was performed at distinct time points after transfer of CFSE-labeled TDLs, with the expectation that cycling immigrants would rapidly engage in proliferation.

At 18 h after transfer, no loss of CFSE was apparent (Fig. 5 B). However, whereas CD44$^{low/int}$ immigrants were CD69$^-$, 30–50% of the CD44^{high} cells already expressed CD69 (unpublished data). At 44 h, decays indicative of 2–4 rounds of division were already observed in a significant fraction of immigrants (Fig. 5 B), especially V$\gamma7^+$ (Fig. 5 C). This burst of proliferation in such short time interval, involving many V$\gamma7^+$ cells, highly represented in the 18 h pool of cycling immigrants (Fig. 4 B), strongly suggested that rapidly dividing cells are the progenies of TDL-derived cycling immigrants.

The frequency of dividing cells and the number of divisions were highest in $\gamma\delta$ immigrants, and lowest in CD4$^+$ immigrants (Fig. 5, B and C). These differences were amplified in the following days (Fig. 5 B), with unconventional cells predominating in late cell division generations (Fig. 5 D). By day 6 after transfer, the $\gamma\delta$/CD4 ratio was 4:1 in the pool of immigrants that divided in situ and resident IELs, as compared with 1:4 in the pool of cycling immigrant at 18 h after transfer (Fig. 5 E).

In summary, the predominance of unconventional over conventional IELs is established in situ due to the higher proliferative potential of the respective cycling TDL precursors.

SI-Ep immigrants acquire high Granzyme B content upon extensive cell division

A large fraction of normal IELs are characterized by cytoplasmic granules containing high amounts of Granzyme B (Guy-Grand et al., 1978, 1991), a feature particular to lymphoid cells displaying strong cytotoxic activity (Tschopp and Nabholz, 1990). In contrast to TDLs or LN cells, essentially all IELs (T and non–T cells, including B cells), expressed detectable levels of Granzyme B (Fig. 6 A), but clusters of these molecules were only observed in CD3$^+$ IELs identified as Granzyme B^{high} in flow cytometry (Fig. 6 B).

We then determined whether TDLs that colonized the SI-Ep had acquired Granzyme B, and whether this process required cell division. As illustrated in Fig. 6 C for $\gamma\delta$ and CD8$\alpha\beta$ cells, the bulk of SI-Ep immigrants expressed Granzyme B at variable levels. Low content of this molecule was already apparent at 18 h after transfer, and it appeared a specific signature of cells that entered the SI-Ep, since immigrants in the SI-LP scored negative (unpublished data). In contrast, high content of Granzyme B correlated with cell division, but only by the fourth generation did the frequency of these cells approach that of host IELs (Fig. 6 C). Granzyme B^{high} cells were 3–4-fold less frequent in CD4 T cell immigrants, in line with their lower proliferative potential (unpublished data).

In conclusion, only cycling immigrants contribute to the pool of highly cytotoxic IELs.

Identification of SI-Ep immigrants and respective progenies in normal IELs at steady state

To validate our transfer system as representative of SI-Ep homing and colonization in physiological conditions, we

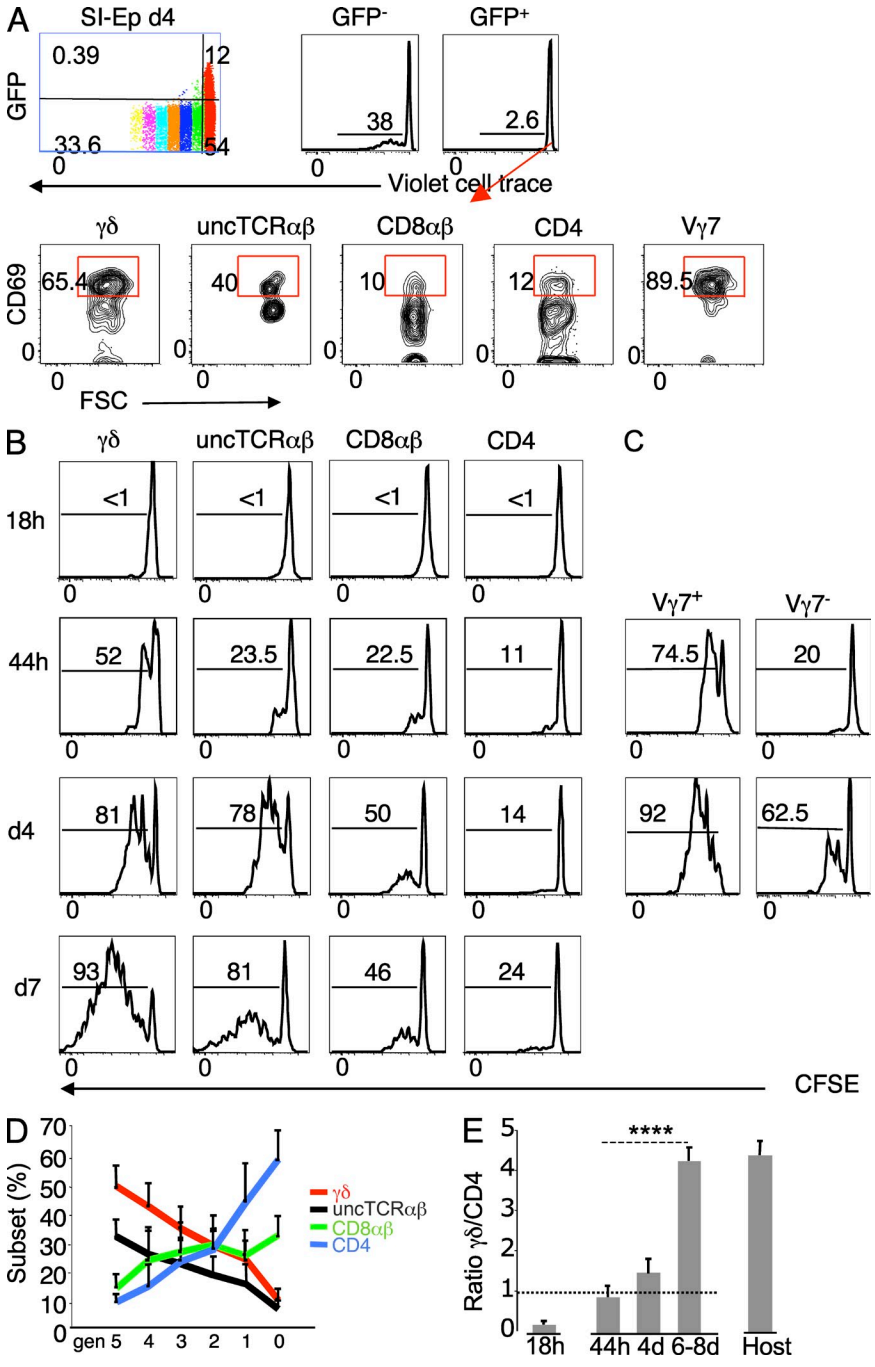

Figure 5. In the SI-Ep, RTEs do not proliferate and cycling unconventional immigrants have the highest proliferation rate. (A) TDLs of 6-wk-old RAG2p-GFP (CD45.2) B6 mice, labeled with violet cell division tracer, were transferred to wild-type CD45.1 B6 mice. Recipients were sacrificed at day 4 post-transfer. (top) Pattern of the violet tracer in donor cells in the SI-Ep and in the respective GFP$^-$ and GFP$^+$ subsets. (bottom) CD69 expression in gated GFP$^+$ immigrants. A second recipient studied in an independent canulation and transfer experiment provided similar results. (B–E) TDLs of 8–12-wk-old (CD45.1) B6 mice labeled with CFSE were transferred to CD45.2 B6 recipients. (B) Kinetics of CFSE patterns of the indicated donor SI-Ep immigrants. The frequencies of the progenies of immigrants that divided one or more times are indicated. Plots are representative of 5–9 independent experiments per time point (total of 30 experiments). Half of the experiments studied 1 recipient and the other half a pool of 2 transferred recipients. (C) Kinetics of CFSE patterns of Vγ7$^+$ and Vγ7$^-$ immigrants as described in B. Plots are representative of two independent transfer experiments, each corresponding to a pool of 2 recipients, per time point. (D) T cell subset distribution at each cell division generation, in the experiments described in B. Since the shift in the distribution correlated with the division generation and not with the time of sacrifice, data correspond to days 4–8 after transfer. (E) γδ/CD4 ratio in immigrants at 18 h after transfer, and in the progenies of immigrants that proliferated in situ, at the indicated time points after transfer, in the transfers described in B, compared with the corresponding ratio in host IELs (n = 46 mice). ****, $P < 0.0001$.

searched for the equivalents to immigrants, and respective progenies, in host IELs.

RTEs in the SI-Ep. In 10-wk-old RAG2p-GFP mice, 1–2% of CD3$^+$ IELs were GFP$^+$ (Fig. 7 A), and most (~60%) expressed CD69. In the CD69$^-$ GFP$^+$ pool, the T cell subset distribution resembled that of RTE immigrants at 18 h after transfer, with a high enrichment of unconventional T cells, though still out-numbered by conventional T cells. In the CD69$^+$ GFP$^+$ pool, unconventional cells predominated, the CD4/CD8αβ ratio was reversed, and the frequency of Vγ7$^+$ cells were 3–4 fold higher (Fig. 7 B). Many CD69$^+$ RTEs were CD44^{high} and displayed typical IELs features, such as CD8αα (Fig. 7 C) and high levels of CD103 (not depicted), but were not cycling (Fig. 7 D). Thus, as in transfers, unconventional RTEs, as well as γδ cells of the Vγ7 family, are preferentially retained and activated in the SI-Ep, but do not proliferate in situ.

To formally show that newly generated T cells of all types reach the SI-Ep shortly after entering circulation,

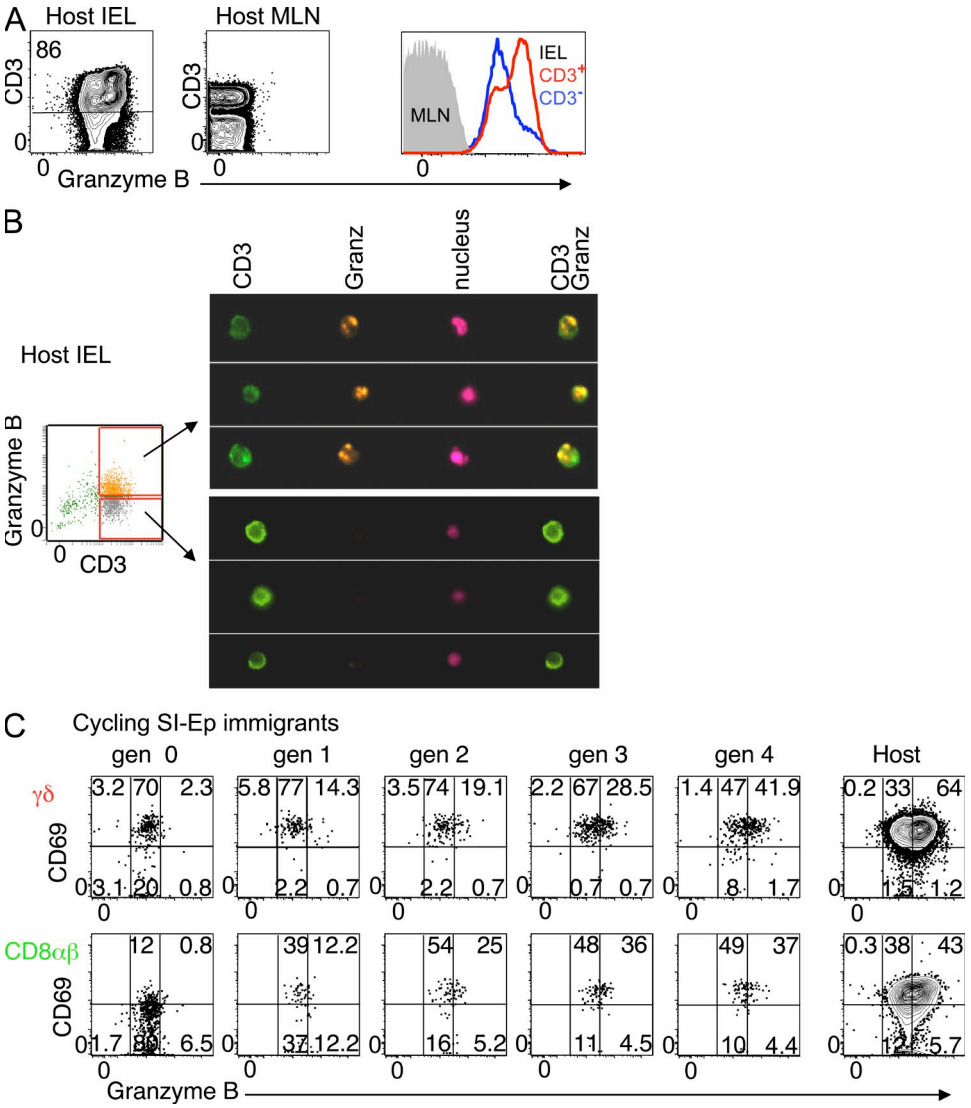

Figure 6. Cycling SI-Ep immigrants are the precursors of Granzyme B^{high} cells. (A) Flow cytometric analysis of the expression levels of Granzyme B in normal IELs and MLNs (15 mice in 15 independent experiments). (B) Structural analysis of Granzyme B content with ImageStream system (Amnis) in the indicated subsets of CD3$^+$ IELs, as defined in the accompanying dot plot (one experiment [preliminary]). (C) Dot plots correlating CD69 expression and levels of Granzyme B in the indicated CFSE generations of donor γδ or CD8αβ SI-Ep immigrants. Data are representative of seven recipients individually analyzed at days 4–8 after transfer, in seven independent experiments.

biotin was injected intrathymically into 4-wk-old RAG2p-GFP mice, and emigrants were tracked 40 h later in the SI-Ep. As shown in Fig. 7 E, avidin-labeled (Av$^+$) GFP$^+$ cells represented ∼0.4% of CD3$^+$ IELs (∼3.0% in LN). Importantly, ∼45% of the Av$^+$ GFP$^+$ cells were γδ$^+$ and ∼3.7% were uncTCRαβ$^+$, as compared, respectively to ∼3% and ∼0.2% in LN. Notably, the T cell subset distribution in avidin$^+$ RTEs (Fig. 7 E) and in CD69$^-$ RTEs immigrants in adults (Fig. 7 B) was comparable, suggesting that homing of RTEs operates similarly at distinct ages of IEL development.

Altogether, these results demonstrate that RTEs of all lineages continuously seed the SI-Ep at steady state, with efficiencies that respect the differences in developmentally determined levels of α4β7 among T cell lineages, as predicted from the transfers.

Cycling SI-Ep immigrants and their progenies. Next, we assessed whether mobile (CD69$^-$) IELs contained cells that might correspond to GALT-related cycling immigrants identified in TDL transfers. CD69$^-$ cells represented ∼7% of CD3$^+$ IELs (Fig. 8 A). Conventional T cells predominated in this pool (Fig. 8 A), which contained the bulk of naive (CD62L^{high} CD44^{low}) IELs (not depicted). Among CD69$^-$ CD3$^+$ IELs, 5–15% were CD44^{high} and expressed Ki-67 and α4β7 (Fig. 8 B). In this pool, the T cell subset distribution and the frequency of Vγ7$^+$ cells were close to those in the

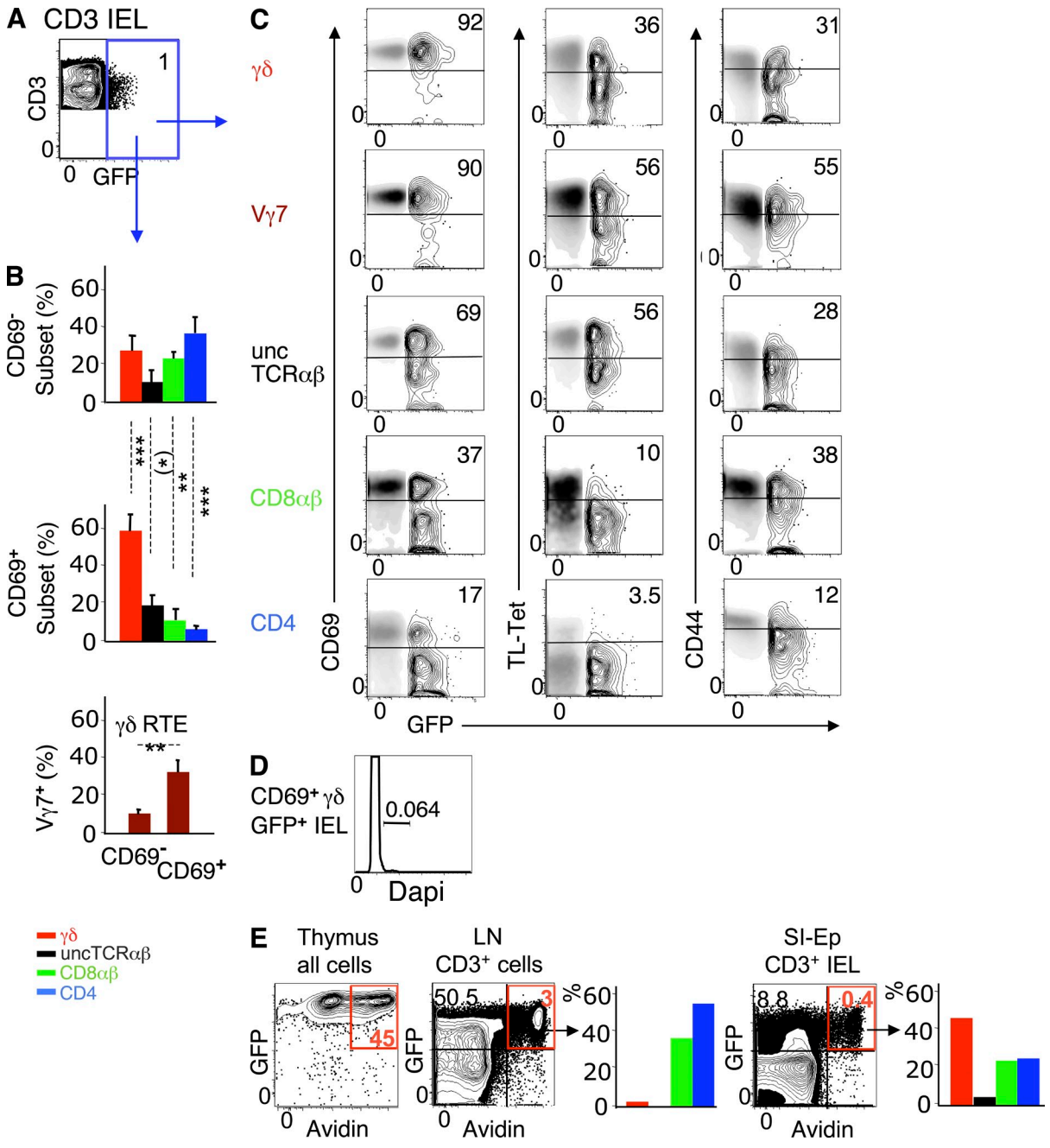

Figure 7. RTEs in normal IELs at steady state. (A) Dot plot correlating CD3 and GFP (RTEs) in IELs of 10-wk-old RAG2p-GFP mice (five mice in five independent experiments). (B) (top and middle) T cell subset distribution in CD69$^-$ and CD69$^+$ GFP$^+$ IELs (same mice as in A). (bottom) Frequency of Vγ7$^+$ cells in CD69$^+$ and CD69$^-$ GFP$^+$ $\gamma\delta$ IELs (four mice in four independent experiments). (C) Gated GFP$^+$ IELs (contour mode) were overlay with GFP$^-$ IELs (density mode) for comparison of the expression levels of the indicated markers (CD8$\alpha\alpha$ expression was detected by TL-tetramer labeling). Inserted numbers (%) relate to the GFP$^+$ subset (same mice as in A). (D) Cell cycle analysis of sorted GFP$^+$ IELs from a pool of six 25-d-old mice (one experiment, [preliminary]). At this age, GFP$^+$ cells were 4.5% of CD3$^+$ IELs. (E) 4-wk-old RAG2p-GFP mice received intrathymically 100 µg of biotin, and were sacrificed 40 h later. Dot plots: frequency of avidin-labeled total thymocytes, and of CD3$^+$ lymphocytes from LN or SI-Ep (red gate). Bar graphs show T cell subset distribution in avidin$^+$ CD3$^+$ cells. Data correspond to two pooled animals. Similar results were obtained with another pool of two mice in an independent experiment.

18-h pool of cycling immigrants in TDL transfers (compare bar graphs of Figs. 8 B and 4 B).

In transfers, cycling SI-Ep immigrants rapidly up-regulated CD69 and engaged in active proliferation (Fig. 5 B), a process that revealed selective advantage of unconventional immigrants, in particular $\gamma\delta^+$ (Fig. 5, C and E). Resident (CD69$^+$) CD3$^+$ IELs also contained CD44^{high} cells coexpressing Ki-67 and $\alpha4\beta7$ (Fig. 8, C and D), whose levels were positively correlated (Fig. 8 D). About one third of $\alpha4\beta7^{high}$ Ki-67^{high} cells were large and had high DNA content (Fig. 8 D),

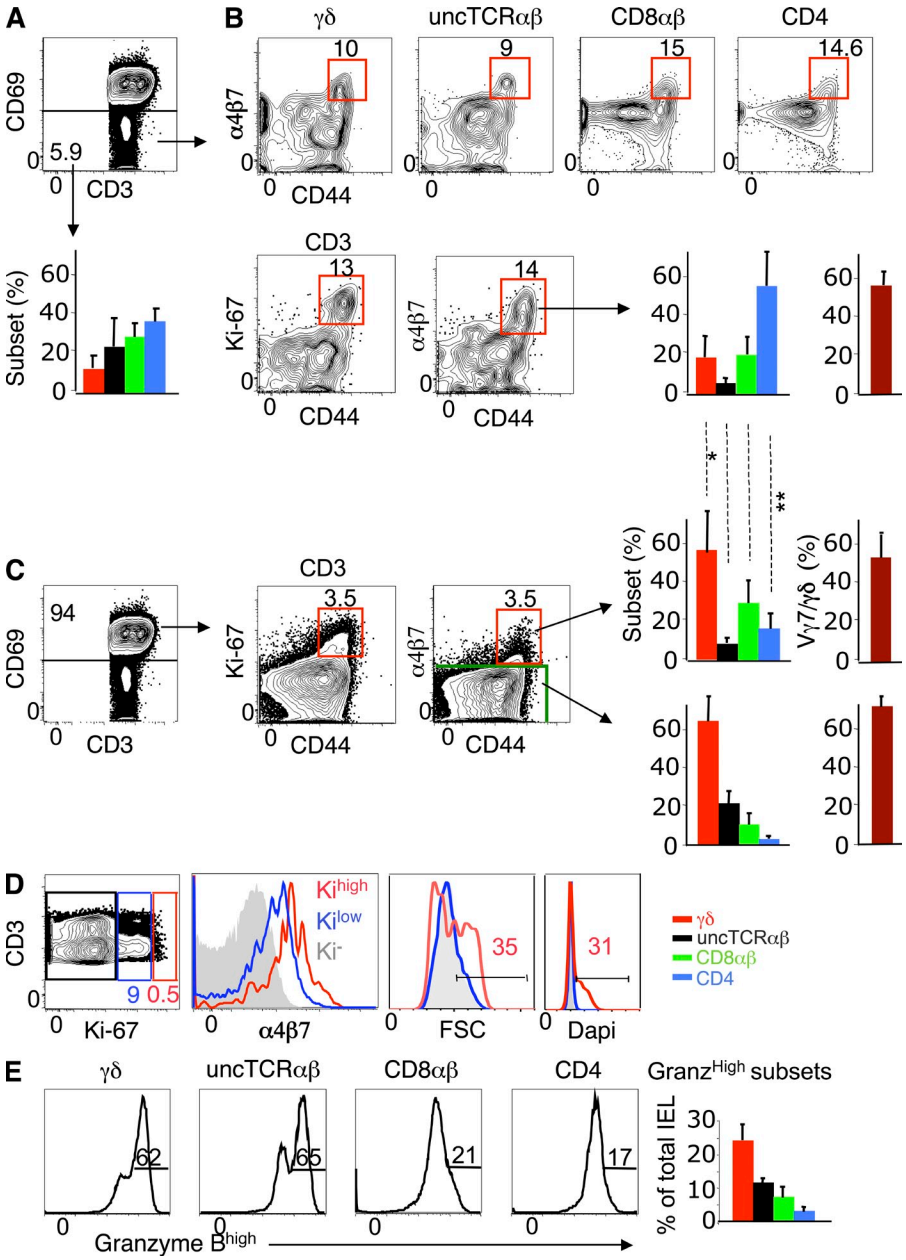

Figure 8. Identification of cycling SI-Ep immigrants, and their progenies, in normal IELs at steady state. (A) Dot plot: Frequency of CD69$^-$ (mobile) cells in CD3$^+$ IELs (mean ± SD: 6.7% ± 4), and corresponding T cell subset distribution (bar graph). Data correspond to 12 mice studied in 12 independent experiments. (B, top) Frequency of α4β7$^+$ CD44^{high} cells in each CD69$^-$ T cell subset (mean ± SD: γδ, 17.3 ± 12.0; uncTCRαβ, 9.8 ± 4.2; CD8αβ, 10.7 ± 4.3; CD4, 10.8 ± 2.5). (bottom) Frequency of Ki-67$^+$ α4β7$^+$ CD44^{high} cells in total CD69$^-$ CD3$^+$ IELs (10.9% ± 4.2), and corresponding T cell subset distribution (bar graph). Frequency of Vγ7$^+$ cells in α4β7$^+$ CD44^{high} Vγδ IELs (right bar graph). Data correspond to 5 mice individually studied in 4 independent experiments. (C) Dot plots show frequency of Ki-67$^+$ α4β7$^+$ CD44^{high} cells in CD69$^+$ (resident) CD3$^+$ IELs (6.9 ± 2.2%), and corresponding T cell subset distribution (bar graph). Frequency of Vγ7$^+$ cells in α4β7$^+$ CD44^{high} γδ IELs (right bar graph). Data correspond to the same experiments in (B). Shown is the statistical significance of CD69$^-$ versus CD69$^+$ α4β7$^+$ CD44^{high} IELs for each T cell subset: *, $P < 0.05$ (γδ); **, $P < 0.05$ (CD4). (D) Dot plot shows the frequency of Ki-67$^{low/int}$ and Ki-67^{high} cells in CD69$^+$ CD3$^+$ IELs (10.6 ± 4.6%). Overlay histogram for α4β7, cell cycle (Dapi) and FSC of gated Ki-67$^{low/int}$ versus Ki-67^{high} CD69$^+$ IELs. Profiles correspond to six mice in six independent experiments, three of which included Dapi. (E) Frequency of Granzyme B^{high} cells in IELs subsets (mean ± SD): γδ, 51.0 ± 10 ($n = 24$); uncTCRαβ, 57.6 ± 7.0 ($n = 6$); CD8αβ, 34.5 ± 14.6 ($n = 15$); CD4, 31.0 ± 14.0 ($n = 11$). One mouse per independent experiment.

which is indicative of active proliferation. In the total pool of Ki-67$^+$ α4β7$^+$ CD69$^+$ cells, the representation of γδ cells was significantly higher than in the corresponding CD69$^-$ pool, whereas that of CD4 T cells was lower (compare bar graphs of Fig. 8, B and C), as expected from the distinct proliferation potential of the respective cycling immigrants (Fig. 5 B,E). Of note, the frequency of CD4 T cells was lowest in Ki-67$^-$ α4β7$^-$ CD69$^+$ IELs (Fig. 8 C, lower bar graph), which compose the vast majority of IELs, suggesting that CD4 T cells do not substantially accumulate as resident IELs. CD4$^+$ IELs also showed the lowest frequency of Granzyme B^{High} cells (Fig. 8 E), which are progenies of migrants that divided extensively (Fig. 6 C). Thus, resident IELs contain cells that resemble the immediate progenies of cycling SI-Ep immigrants in transfer experiments.

In conclusion, the heterogeneity of normal IELs reflected the main steps of SI-Ep colonization followed by transferred TDLs.

SI-Ep immigrants contribute significantly to the dynamics of IELs at steady state

The SI-Ep is considered of low accessibility to newly coming immigrants because of the large number and long lifespan of resident IELs, hence the lack of available niches.

Based on the transfer experiments, we estimated the quantitative impact of the progenies of circulating cells, entering the SI-Ep every 18 h, on the respective IEL populations (Table 2, see legend for detailed information). The results are primarily built upon the estimation that the number of T cells

entering the SI-Ep during that period is ∼5% (2.5 million cells) of resident IELs. However, as detailed for each T cell subset in the following paragraphs, most immigrants will not establish interactions in situ, and hence, the number of circulating cells integrating the SI-Ep is low.

Because T cell subsets are distinctly distributed in SI-Ep immigrant and resident IEL populations, and naive and cycling immigrants have distinct reactivity to local cues and proliferation potential, the impact of the daily cohort of immigrants differed significantly between cell types.

For γδ T cells, 40–50% of IELs, the daily cohort of immigrants was ∼1% of the respective resident population, but those with potential of integration only represented ∼0.3%, of which one third were GALT-related cycling cells. In about 1 wk, the immigrant population accounted for ∼3% of all γδ IELs, >90% of which were progenies of immigrants that expanded in situ. These results suggest that, if no other selective events operate (e.g., competition for survival), the progenies of cells continuously seeding the SI-Ep might generate in ∼38 d a number equivalent to that of the resident IEL population. That is, the average life span of this pool could be ∼38 d (Table 2). As also shown, similar estimations were obtained for uncTCRαβ IELs.

For CD4 T cells, ∼10% of IELs, daily immigrants were ∼25% of the respective resident population, and those with potential of integration ∼4%, of which two thirds were cycling. In ∼4 d, these immigrants generated a population accounting for ∼10% of CD4 IELs, 80% of which were the progenies of cycling immigrants. Thus, the CD4 IELs might be entirely renewed in ∼14 d and CD8αβ IELs in ∼20 d (Table 2).

In conclusion, despite their low number, circulating GALT-related cycling T cells have a high capacity of SI-Ep colonization, thereby contributing to the dynamics of normal IELs.

DISCUSSION

Based on a quantitative description of the natural history of SI-Ep tropic conventional and unconventional T cells, we show that all T cell subsets follow the same general rules of homing and colonization of the SI-Ep, and that in adult physiological conditions, circulating cells continuously colonize this tissue, contributing to the dynamics of resident IELs. This integrated view is schematized in Fig. S1.

The common homing pattern of T cell subsets reflected similarities in acquisition of gut-tropic molecules during development in the thymus, and in the reenforcement of the expression of these molecules upon immune responses in the GALT.

With respect to development, the key findings were that newly generated T cells of all lineages, identified by the recent expression of the RAG-2 gene, share two major general properties: they leave the thymus in a naive state, and are endowed with the dual capacity of circulating through secondary lymphoid organs and the SI. However, whereas conventional RTEs, which express low levels of α4β7 and high levels of CD62L, circulate preferentially through lymphoid organs, unconventional RTEs, which express high levels of both molecules, have no preference between the secondary lymphoid organs and the SI.

Table 2. Dynamics of SI-Ep homing and colonization at steady state

	Input per 18h[a] (% of the respective IEL subset)			Progenies of the18h-input[e] (% of the respective IELs sub.)		Resident IELs
	Total[b]	Retained in situ[c]	Ratio naive versus cycling[d]	Total[f]	Ratio undivided versus divided[g]	Average life-span of IELs (days)[h]
γδ	∼1.0	0.3	2:1	∼3.3	1:15	38 (33–43)
UncTCRαβ	∼2.0	0.4	1:1	∼3.5	1:13	34 (26–39)
CD8	∼6.0	0.8	1:3	∼8.0	1:12	19 (12–32)
CD4	∼25.0	3.6	1:2	∼10.0	1:5	14 (12–16)

[a]At 18 h after transfer, the average frequency of donor CD3+ TDLs was ∼10% of CD3+ cells in peripheral lymphoid organs and blood, and ∼0.5% in the SI-Ep (Fig. 4 A). Assuming that the donor population was an unbiased representation of host circulating T cells, then the total number of cells (donor plus host) entering the SI-Ep during that period was ∼5% of IELs. This estimation is close to the frequency of CD69− cells (∼6%) in CD3+ IELs, a result that supports the above assumption.

[b]In the 18-h SI-Ep immigrant pool, ∼11% were γδ+, ∼7% uncTCRαβ, ∼24% CD8+ and ∼53% CD4+ (Fig. 4 A). These values were referred to the 5% input per 18 h, and then to the average frequency of each T cell subset in IELs (Table 1).

[c]The estimation of the frequency of immigrants retained in the SI-Ep was based on the frequency of donor cells that expressed CD69 at 44 h after transfer. For naïve immigrants (based on the analysis of RTEs), the percentage of CD69+ cells in each T cell subset were as follows: γδ+, 19.6%; uncTCRαβ, 13.3%; CD8+, 3.2%; CD4+, 4.9%. For cycling immigrants, >90% expressed CD69 in all T cell subsets. These values were then referred to the frequency of naive and cycling cells in the 18-h pool of immigrants, which were ∼90% and ∼10%, respectively, in all subsets (Fig. 4B).

[d]These ratios were determined from the estimations of the number of naive and cycling immigrants retained in situ as described in c.

[e]We designate as progenies of the 18-h input all donor immigrants that expressed CD69 by days 4 to 8 after transfer, regardless of whether they had proliferated or not.

[f]The number of donor CD69+ cells in the SI-Ep was maximal by day 4 after transfer, and remained stable up to day 8 after transfer, except for γδ, whose maximal values were reached by days 6 to 8. The estimations were based on the analysis of 9 individually studied recipients.

[g]Ratios between undivided cells and the progenies of cells that had proliferated, were estimated based on the CFSE profiles, of which representative examples are shown in Fig. 7, and take into account that only a fraction of the undivided cells expressed CD69, while this molecule was expressed by >90% of proliferating cells.

[h]The average life span corresponds to values estimated in footnote f, to which the time period necessary to reach maximal values was added (about 7 d for γδ cells and 4 d for all the other subsets). Ranges are indicated in parenthesis.

In regard to developing TCRγδ cells, acquisition of α4β7 is thus neither associated with high-strength TCR signaling, as shown for a minor subset of SI-Ep–tropic γδ T cells (Jensen et al., 2009), nor with any other process restricting its expression to specific TCRγ families. This was demonstrated by the high SI-Ep tropism of Vγ4 cells that are poorly represented in resident IELs. Therefore, γδ development in the adult follows rules distinct from those in the fetus, characterized by the strict association of TCR Vγ families and homing to specific tissues (e.g., Vγ5 and skin). Moreover, the fact that major Vδ families are similarly expressed by Vγ7$^+$ cells in thymus, LNs, and IELs (Pereira et al., 2000) suggests that SI-Ep tropism is also a general property of cells expressing this Vγ family. As such, TCRγδ RTEs migrate to the SI-Ep in a TCR repertoire–independent fashion and without selection for ligands expressed in this tissue. Thus, the predominance of Vγ7$^+$ cells in IELs is not developmentally determined.

The evaluation of SI-Ep tropism in the general context of lymphocyte recirculation showed that many unconventional RTEs prone to colonize the SI-Ep travel through the hemolymphatic system before being eventually arrested in the SI-Ep, as indicated by the high number of (SI-tropic) Vγ7$^+$ RTEs recovered from the thoracic duct, or present in PLNs and MLNs. The functional relevance of this traffic pattern became apparent with the recognition of the GALT as central sites of unconventional T cell activation, coupled to strong upregulation of α4β7 and CCR9, as known for conventional T cells. The concomitant loss of CD62L indicated that the corresponding cycling blasts, identified in the thoracic duct, have been reprogrammed to migrate (almost) exclusively to the SI wall.

The high enrichment of Vγ7$^+$ cells in cycling γδ blasts in MLNs, but not PLNs, suggests a strong link between GALT-selected and IEL repertoires, as demonstrated for CD8αβ T cells (Arstila et al., 2000). This link argues against compartmentalization of peripheral versus IEL TCRγδ T cells as exclusive, nonoverlapping populations (Chennupati et al., 2010). The finding that most Vγ7$^+$ blasts in circulation expressed gut-tropic molecules indicated that the GALT is the main peripheral territory where cells of this Vγ family are activated. This raises the issue of where in the GALT Vγ7$^+$ TDL blasts are generated, as the respective ligands are supposedly confined to the SI-Ep. In MLNs, cycling blasts did not display signs of retention, indicating that dendritic cells traveling from the SI wall to MLN (Farache et al., 2013) do not seem to carry antigens recognized by Vγ7$^+$ T cells. PPs, whose structures include a layer of epithelial cells, contained both CD69$^+$ and CD69$^-$ Vγ7$^+$ blasts, but in-depth dynamic studies are necessary to formally show that Vγ7$^+$ RTEs activated to cycle in PPs are precursors of the Vγ7$^+$ cycling blasts that migrate through MLNs to the thoracic duct. Isolated lymphoid follicles in the SI-LP might be another source of these cells, as these structures share properties with PPs and are also in close contact with the SI-Ep (Cauley and Lefrançois 2013).

With respect to rules governing SI-Ep colonization under steady-state conditions, our studies provide two major findings.

First, despite their low frequency, GALT-related cycling immigrants are the major source of IELs, because they have a much higher retention and proliferation dynamics than naive immigrants. The preferential retention of cycling immigrants is best explained by the strong repertoire selection operating in the GALT, and not in the thymus. Indeed, although the SI-Ep environment might provide TCR-independent signals leading to cell arrest (Casey et al., 2012), the crucial triggering event appears to be TCR-mediated, as suggested by the selective retention and activation of Vγ7$^+$ cells among naive γδ immigrants. In contrast to cycling immigrants, naive immigrants activated in situ have a poor proliferation potential, for reasons still unknown. Therefore, they only contribute to the respective IEL subsets by accumulation and do not differentiate into Granzyme B^{high} effectors, which require extensive proliferation in situ. If secretion of cytokine or antibacterial peptide does not require cell division, these might be functions of naive immigrants, whereas cycling immigrants are the sole precursors of Granzyme B^{high} IELs. Thus, priming in the GALT is a necessary step for the development of cytolytic responses in the intestinal mucosa.

Second, circulating cells have a very high capacity of short-term colonization of the SI-Ep under steady-state conditions, despite the very large number of resident IELs. As shown in this study, the few immigrants entering the SI-Ep every 18 h, in particular those cycling (∼0.4% of IELs), generated in a short period of time (4 to 7 d) progenies accounting for 3% unconventional to 8–10% conventional cells of the respective resident IEL subsets. These results argue against the idea that the SI-Ep is a site of restricted accessibility.

These results suggest average life spans of resident IELs of ∼30 to 40 d for unconventional and 15 to 20 d for conventional IELs. However, it should be noted that, being averages, these estimations do not preclude that a fraction of IELs might be long-lived (Chennupati et al., 2010), and that, likely, other selective events might operate, namely in situ competition for survival. Indeed, although the size of the progenies of the 18 h cohort of γδ immigrants stabilized by the first week after transfer, a fraction of them continued to divide (unpublished data), implying concomitant death of other cells. Thus, cell death appears to play an important role in IEL homeostasis. Because survival of γδ and uncTCRαβ IELs requires signaling through the Aryl Hydrocarbon receptor (Li et al., 2011), competition for its ligand could play a physiological role in the intraepithelial selection of the most fitted clones. Thus, "resident" IELs might be composed of clones with heterogeneous life spans, leaving room to the continuous integration of new gut-tropic cycling T cells developed upon on-going natural immune responses in the GALT. Indeed, in specific immune responses, most CD8 cells that seed the SI-Ep had a relatively short life span (Masopust et al., 2001).

Our estimations on life spans appear difficult to reconcile with the slow rate of redistribution of IELs in the SI-Ep of parabionts (Poussier et al., 1992). These authors found that, by day 38 post-surgical joining, the maximal exchange between partners was ∼13% T cell chimerism in the SI-Ep (without

distinction between subsets), as compared with ∼50% in LNs. Correcting for lag times required for the full establishment of anastomosis (∼8 d) and the development of immune responses in the GALT (∼7 d), this chimerism was in fact ∼13% in 23 d. This would suggest (correcting for the 50% expected chimerism if access to the SI-Ep was unrestricted) an average life span of 100 d. The gap left between these and our estimations might, for the most part, be explained by severe thymic involution caused by surgical stress, which particularly impacts the dynamics of SI-Ep–tropic unconventional T cells, which are highly dependent on continuous thymic output. Studies involving parabiosis or intestinal grafts (Klonowski et al., 2004; Masopust et al., 2010), showing that memory T cells have poor SI-Ep tropism, are explained by the observation that up-regulation of α4β7 is transient (Masopust et al., 2010).

Our studies offer explanations for the predominance of unconventional T cells in IELs of SPF mice. One is the 10-fold higher proportion of both naive and cycling cells homing to the SI-Ep. Whereas for naive cells this is due to higher levels of tropic molecules, for cycling cells this is likely due to a higher frequency of antigen-reactive cells in the GALT (particularly cells of the Vγ7 family), and also that many CD4 T cells up-regulate α4β7 and not CCR9, and hence will preferentially be retained in the SI-LP. Other reasons are the higher rate of retention of unconventional naive immigrants (caused by higher frequency of antigen-reactive cells), and the higher proliferation dynamics of unconventional cycling immigrants, for reasons still unclear. The estimated differences in average life span of IEL subsets suggest that survival rates may also influence the respective homeostasis, in line with the observation that unconventional IELs express the highest levels of the antiapoptotic factor BCL2 (Van Houten et al., 1997). Finally, the reversed CD4/CD8αβ ratio in normal IELs is best explained by the distinct proliferation dynamics of the respective cycling immigrants, although it should be pointed out that unconventional and conventional IELs do not compete for the same niches (Bandeira et al., 1990; Li et al., 2011), and that in mice kept in conventional conditions or in humans, conventional IELs predominate. Even in this case, conventional cells expand predominantly in the GALT and not in the SI-Ep (unpublished data).

Although we confirm the major role of α4β7 in SI-Ep homing, this is less clear for CCR9. First, a sizeable number of naive CD4 T cells, which lack CCR9, enter the SI-Ep every day. Second, blocking α4β7 drastically reduced the number of γδ T cells and cycling immigrants of all types, despite their high levels of CCR9. Thus, this molecule might instead contribute to retention in the SI-Ep.

In conclusion, our study demonstrates that although tropism for the SI-Ep is imprinted during thymic development, the immune system developed strategies that maximize the continuous influx to the SI-Ep of both conventional and unconventional cells capable of rapid proliferation and differentiation in situ into cytotoxic effectors. Our quantitative analyses help define the fundamental principles that guide trafficking and colonization of the SI-Ep under physiological conditions.

MATERIALS AND METHODS

Mice. CD45.1 and CD45.2 C57BL/6 mice were purchased from Charles River and kept in specific pathogen–free conditions in our house facilities. FVB RAG2p-GFP mice (Yu et al., 1999) were backcrossed into C57BL/6 mice for 13 generations, now designated as RAG2p-GFP C57BL/6 mice. Mice were cared for in accordance with Pasteur Institute guidelines in compliance with European animal welfare regulations, and all experimental studies were approved by the Pasteur Institute Safety committee in accordance with French and European guidelines and by the ethics Committee of Paris I (permits 2013–0002, 2010–0003, 2010–0004; permit 2005–0003 for thoracic duct canulations).

Canulation of the thoracic duct. 6 wk–5 mo-old mice were anesthetized and their thoracic ducts were exposed behind the left kidney. A carefully heat-curved polythene catheter (0.40 mm ID, 0.80 OD or 0.58 mm ID, 0.96 OD, depending on the size of the mouse; Portex UK) was inserted into the duct beneath the diaphragm, glued with Histoacryl (Braun), and exteriorized at the lower part of the ventral incision. Mice received 0.7 ml phosphate-buffer-saline per hour, via the tail vein, using an infusion pump (Harvard Apparatus). They were kept overnight on hamster wheels, which rotated periodically. Lymph was collected in ice-cold culture medium containing heparin. The average number of TDLs recovered during 20 h was 43×10^6 (±26) per mouse, and $50–60 \times 10^6$ TDLs were intravenously injected in the recipients.

Isolation of mucosal lymphocytes. The SI was flushed with PBS, and PPs were carefully removed. The intestine was opened and cut into 1-cm pieces. For IEL isolation, these fragments were incubated in 50 ml RPMI 1640 (Invitrogen) with 10% FCS, at 37.5° with 5% CO_2, under strong magnetic stirring for 1 h, followed by strong vortex. To eliminate epithelial cells, the supernatant was filtered through a buffered glass wool column (1 g of short fibers of borosilicated glass wool; Thermo Fisher Scientific) packed into a 20-ml syringe. For LPL isolation, the fragments were first incubated for 15 min at 37° with magnetic stirring in 50 ml Hanks' balanced salt solution without $CaCl_2$ and $MgCl_2$, with 0.5 mM EDTA (Sigma-Aldrich), then twice in medium without EDTA. When the supernatant became clear, the fragments were incubated in 50 ml RPMI 1640 with 20% FCS and 2.5 mg collagenase (C2139; Sigma-Aldrich) for 20 min. To complete digestion, the medium was mixed with a 10-ml syringe for 5 min. Finally, IEL or LPL suspensions were filtered through a 40-µm cell strainer (BD), and then dispersed in 70% Percoll (GE Healthcare) overlaid with 40% Percoll and centrifuged 10mn at 2200 RPM without brake. Lymphocytes were collected at the interface. Routinely, $10–30 \times 10^6$ IELs or LPLs were collected per mouse.

In vivo mAb treatment. Anti-α4β7 mAb was purified by affinity chromatography using HiTrap Protein G column (GE Healthcare). TDLs were incubated for 30 min with 200 µg of the mAb, and the preparation was injected into the recipients.

Intrathymic injections of biotin. The use of biotin to track thymic emigrants was first performed by Carlson et al. (2006). 100 µg of biotinamidohexanoic acid3-sulfo-N-hydroxysuccinimide ester sodium salt (Sigma-Aldrich) were injected into thymic lobes of anesthetized mice after a small incision of the sternum.

Flow cytometry. For CFSE or Violet stain (Invitrogen) cell tracer labeling, 10^7/ml TDLs were incubated in PBS+3% FCS and 5 µM cell tracer for 10mn at 37.5°C with gentle stirring. For cell surface staining, fluorescent mAbs were purchased from BD, eBioscience, or BioLegend. Anti-CCR9 was obtained from R&D systems. TL tetramers were prepared as described (Pardigon et al., 2004). For intracellular staining of Granzyme B (anti–human Granzyme B; Invitrogen) or Ki-67 (anti–human Ki-67; BD), cells were fixed and permeabilized with kits from BD and eBioscience, respectively. Dead cells were excluded by labeling with Aqua Dead cell stain kit (Molecular Probes). Samples with 7–8 fluorochromes were analyzed with a FACSCanto

(BD) and FlowJo software (Tree Star). The cell tracer profiles were studied with the specific FlowJo program. GFP$^+$ TDLs were sorted in a MoFlo Cytomation (Beckmann Coulter) with a purity of 97.7%.

Determination of the total number of CD3$^+$ cells per organ. Values were calculated as follows: Spleen, 20 million; total LN, 45 million (twice the sum of MLN, axillary, brachial, and inguinal LN cells; Zatz and Lance, 1970). IELs were 50 million (Rocha et al, 1991). LPLs were 35 million, as assessed from tissue sections with the methodology described for IELs (Rocha et al, 1991).

Statistical analysis. Data were calculated as mean ± SD. Statistical significance was performed using two-tailed Student's *t* test with 95% confidence intervals, under the assumption of equal variances between groups.

Online supplemental material. Fig. S1 shows the hemolymphatic cycle of gut-tropic T cells. Online supplemental material is available at http://www.jem.org/cgi/content/full/jem.20122588/DC1.

We thank Eugène Butcher for providing the anti-α4β7 antibody, Brian Hall (Amnis corporation) for structural analysis with ImageStream system (Amnis), B. Jabri, L. Peduto, B. Silva-Santos, and H. Strick-Marchand for discussions, and members of our laboratories for technical help and discussion.

The work was supported by funds of the Fondation ARC (n°1007) to A.B., La Ligue Contre le Cancer Comité de Paris and the Labex REVIVE to A. Cumano, ANR Blanc 'Gut ILC' to J.P. Di Santo, FP7 ERC "QSIS" n°249740 to A.A. Freitas, and funds from Pasteur, Centre National de la Recherche Scientifique, and Institut National de la Santé et de la Recherche Médicale.

The authors have no conflicting financial interests.

Submitted: 22 November 2012
Accepted: 3 July 2013

REFERENCES

Arstila, T., T.P. Arstila, S. Calbo, F. Selz, M. Malassis-Seris, P. Vassalli, P. Kourilsky, and D. Guy-Grand. 2000. Identical T cell clones are located within the mouse gut epithelium and lamina propia and circulate in the thoracic duct lymph. *J. Exp. Med.* 191:823–834. http://dx.doi.org/10.1084/jem.191.5.823

Bandeira, A., T. Mota-Santos, S. Itohara, S. Degermann, C. Heusser, S. Tonegawa, and A. Coutinho. 1990. Localization of γ/δ T cells to the intestinal epithelium is independent of normal microbial colonization. *J. Exp. Med.* 172:239–244. http://dx.doi.org/10.1084/jem.172.1.239

Bankovich, A.J., L.R. Shiow, and J.G. Cyster. 2010. CD69 suppresses sphingosine 1-phosophate receptor-1 (S1P1) function through interaction with membrane helix 4. *J. Biol. Chem.* 285:22328–22337. http://dx.doi.org/10.1074/jbc.M110.123299

Berlin, C., E.L. Berg, M.J. Briskin, D.P. Andrew, P.J. Kilshaw, B. Holzmann, I.L. Weissman, A. Hamann, and E.C. Butcher. 1993. α 4 β 7 integrin mediates lymphocyte binding to the mucosal vascular addressin MAdCAM-1. *Cell.* 74:185–195. http://dx.doi.org/10.1016/0092-8674(93)90305-A

Boursalian, T.E., J. Golob, D.M. Soper, C.J. Cooper, and P.J. Fink. 2004. Continued maturation of thymic emigrants in the periphery. *Nat. Immunol.* 5:418–425. http://dx.doi.org/10.1038/ni1049

Carlson, C.M., B.T. Endrizzi, J. Wu, X. Ding, M.A. Weinreich, E.R. Walsh, M.A. Wani, J.B. Lingrel, K.A. Hogquist, and S.C. Jameson. 2006. Kruppel-like factor 2 regulates thymocyte and T-cell migration. *Nature.* 442:299–302. http://dx.doi.org/10.1038/nature04882

Casey, K.A., K.A. Fraser, J.M. Schenkel, A. Moran, M.C. Abt, L.K. Beura, P.J. Lucas, D. Artis, E.J. Wherry, K. Hogquist, et al. 2012. Antigen-independent differentiation and maintenance of effector-like resident memory T cells in tissues. *J. Immunol.* 188:4866–4875. http://dx.doi.org/10.4049/jimmunol.1200402

Cauley, L.S., and L. Lefrançois. 2013. Guarding the perimeter: protection of the mucosa by tissue-resident memory T cells. *Mucosal Immunol.* 6:14–23. http://dx.doi.org/10.1038/mi.2012.96

Chennupati, V., T. Worbs, X. Liu, F.H. Malinarich, S. Schmitz, J.D. Haas, B. Malissen, R. Förster, and I. Prinz. 2010. Intra- and intercompartmental movement of gammadelta T cells: intestinal intraepithelial and peripheral gammadelta T cells represent exclusive nonoverlapping populations with distinct migration characteristics. *J. Immunol.* 185:5160–5168. http://dx.doi.org/10.4049/jimmunol.1001652

Cheroutre, H., F. Lambolez, and D. Mucida. 2011. The light and dark sides of intestinal intraepithelial lymphocytes. *Nat. Rev. Immunol.* 11:445–456. http://dx.doi.org/10.1038/nri3007

Farache, J., I. Koren, I. Milo, I. Gurevich, K.-W. Kim, E. Zigmond, G.C. Furtado, S.A. Lira, and G. Shakhar. 2013. Luminal bacteria recruit CD103+ dendritic cells into the intestinal epithelium to sample bacterial antigens for presentation. *Immunity.* 38:581–595. http://dx.doi.org/10.1016/j.immuni.2013.01.009

Gangadharan, D., F. Lambolez, A. Attinger, Y. Wang-Zhu, B.A. Sullivan, and H. Cheroutre. 2006. Identification of pre- and postselection TCRalphabeta+ intraepithelial lymphocyte precursors in the thymus. *Immunity.* 25:631–641. http://dx.doi.org/10.1016/j.immuni.2006.08.018

Goodman, T., and L. Lefrancois. 1989. Intraepitheliallymphocytes. Anatomical site, not T cell receptor form, dictates phenotype and function. *J. Exp. Med.* 170:1569–1581. http://dx.doi.org/10.1084/jem.170.5.1569

Guy-Grand, D., and P. Vassalli. 1986. Gut injury in mouse graft-versus-host reaction. Study of its occurrence and mechanisms. *J. Clin. Invest.* 77:1584–1595. http://dx.doi.org/10.1172/JCI112474

Guy-Grand, D., C. Griscelli, and P. Vassalli. 1978. The mouse gut T lymphocyte, a novel type of T cell. Nature, origin, and traffic in mice in normal and graft-versus-host conditions. *J. Exp. Med.* 148:1661–1677. http://dx.doi.org/10.1084/jem.148.6.1661

Guy-Grand, D., M. Malassis-Seris, C. Briottet, and P. Vassalli. 1991. Cytotoxic differentiation of mouse gut thymodependent and independent intraepithelial T lymphocytes is induced locally. Correlation between functional assays, presence of perforin and granzyme transcripts, and cytoplasmic granules. *J. Exp. Med.* 173:1549–1552. http://dx.doi.org/10.1084/jem.173.6.1549

Guy-Grand, D., B. Cuénod-Jabri, M. Malassis-Seris, F. Selz, and P. Vassalli. 1996. Complexity of the mouse gut T cell immune system: identification of two distinct natural killer T cell intraepithelial lineages. *Eur. J. Immunol.* 26:2248–2256. http://dx.doi.org/10.1002/eji.1830260942

Guy-Grand, D., O. Azogui, S. Celli, S. Darche, M.C. Nussenzweig, P. Kourilsky, and P. Vassalli. 2003. Extrathymic T cell lymphopoiesis: ontogeny and contribution to gut intraepithelial lymphocytes in athymic and euthymic mice. *J. Exp. Med.* 197:333–341. http://dx.doi.org/10.1084/jem.20021639

Hamann, A., D.P. Andrew, D. Jablonski-Westrich, B. Holzmann, and E.C. Butcher. 1994. Role of α 4-integrins in lymphocyte homing to mucosal tissues in vivo. *J. Immunol.* 152:3282–3293.

Heilig, J.S., and S. Tonegawa. 1986. Diversity of murine γ genes and expression in fetal and adult T lymphocytes. *Nature.* 322:836–840. http://dx.doi.org/10.1038/322836a0

Iwata, M., A. Hirakiyama, Y. Eshima, H. Kagechika, C. Kato, and S.Y. Song. 2004. Retinoic acid imprints gut-homing specificity on T cells. *Immunity.* 21:527–538. http://dx.doi.org/10.1016/j.immuni.2004.08.011

Jensen, K.D., S. Shin, and Y.H. Chien. 2009. Cutting edge: Gammadelta intraepithelial lymphocytes of the small intestine are not biased toward thymic antigens. *J. Immunol.* 182:7348–7351. http://dx.doi.org/10.4049/jimmunol.0900465

Klonowski, K.D., K.J. Williams, A.L. Marzo, D.A. Blair, E.G. Lingenheld, and L. Lefrançois. 2004. Dynamics of blood-borne CD8 memory T cell migration in vivo. *Immunity.* 20:551–562. http://dx.doi.org/10.1016/S1074-7613(04)00103-7

Lafaille, J.J., A. DeCloux, M. Bonneville, Y. Takagaki, and S. Tonegawa. 1989. Junctional sequences of T cell receptor γ δ genes: implications for γ δ T cell lineages and for a novel intermediate of V-(D)-J joining. *Cell.* 59:859–870. http://dx.doi.org/10.1016/0092-8674(89)90609-0

Lefrançois, L., C.M. Parker, S. Olson, W. Muller, N. Wagner, M.P. Schön, and L. Puddington. 1999. The role of β7 integrins in CD8 T cell trafficking during an antiviral immune response. *J. Exp. Med.* 189:1631–1638. http://dx.doi.org/10.1084/jem.189.10.1631

Li, Y., S. Innocentin, D.R. Withers, N.A. Roberts, A.R. Gallagher, E.F. Grigorieva, C. Wilhelm, and M. Veldhoen. 2011. Exogenous stimuli maintain intraepithelial lymphocytes via aryl hydrocarbon receptor activation. *Cell*. 147:629–640. http://dx.doi.org/10.1016/j.cell.2011.09.025

Masopust, D., V. Vezys, A.L. Marzo, and L. Lefrançois. 2001. Preferential localization of effector memory cells in nonlymphoid tissue. *Science*. 291:2413–2417. http://dx.doi.org/10.1126/science.1058867

Masopust, D., D. Choo, V. Vezys, E.J. Wherry, J. Duraiswamy, R. Akondy, J. Wang, K.A. Casey, D.L. Barber, K.S. Kawamura, et al. 2010. Dynamic T cell migration program provides resident memory within intestinal epithelium. *J. Exp. Med*. 207:553–564. http://dx.doi.org/10.1084/jem.20090858

Mora, J.R., M.R. Bono, N. Manjunath, W. Weninger, L.L. Cavanagh, M. Rosemblatt, and U.H. Von Andrian. 2003. Selective imprinting of gut-homing T cells by Peyer's patch dendritic cells. *Nature*. 424:88–93. http://dx.doi.org/10.1038/nature01726

Müller, S., M. Bühler-Jungo, and C. Mueller. 2000. Intestinal intraepithelial lymphocytes exert potent protective cytotoxic activity during an acute virus infection. *J. Immunol*. 164:1986–1994.

Pardigon, N., S. Darche, B. Kelsall, J.R. Bennink, and J.W. Yewdell. 2004. The TL MHC class Ib molecule has only marginal effects on the activation, survival and trafficking of mouse small intestinal intraepithelial lymphocytes. *Int. Immunol*. 16:1305–1313. http://dx.doi.org/10.1093/intimm/dxh133

Pereira, P., V. Hermitte, M.P. Lembezat, L. Boucontet, V. Azuara, and K. Grigoriadou. 2000. Developmentally regulated and lineage-specific rearrangement of T cell receptor Valpha/δ gene segments. *Eur. J. Immunol*. 30:1988–1997.

Poussier, P., P. Edouard, C. Lee, M. Binnie, and M. Julius. 1992. Thymus-independent development and negative selection of T cells expressing T cell receptor α/β in the intestinal epithelium: evidence for distinct circulation patterns of gut- and thymus-derived T lymphocytes. *J. Exp. Med*. 176:187–199. http://dx.doi.org/10.1084/jem.176.1.187

Rocha, B., P. Vassalli, and D. Guy-Grand. 1991. The V β repertoire of mouse gut homodimeric α CD8+ intraepithelial T cell receptor α/β + lymphocytes reveals a major extrathymic pathway of T cell differentiation. *J. Exp. Med*. 173:483–486. http://dx.doi.org/10.1084/jem.173.2.483

Shiow, L.R., D.B. Rosen, N. Brdicková, Y. Xu, J. An, L.L. Lanier, J.G. Cyster, and M. Matloubian. 2006. CD69 acts downstream of interferon-α/β to inhibit S1P1 and lymphocyte egress from lymphoid organs. *Nature*. 440:540–544. http://dx.doi.org/10.1038/nature04606

Staton, T.L., A. Habtezion, M.M. Winslow, T. Sato, P.E. Love, and E.C. Butcher. 2006. CD8+ recent thymic emigrants home to and efficiently repopulate the small intestine epithelium. *Nat. Immunol*. 7:482–488. http://dx.doi.org/10.1038/ni1319

Stock, A., G. Napolitani, and V. Cerundolo. 2013. Intestinal DC in migrational imprinting of immune cells. *Immunol. Cell Biol*. 91:240–249. http://dx.doi.org/10.1038/icb.2012.73

Tschopp, J., and M. Nabholz. 1990. Perforin-mediated target cell lysis by cytolytic T lymphocytes. *Annu. Rev. Immunol*. 8:279–302. http://dx.doi.org/10.1146/annurev.iy.08.040190.001431

Van Houten, N., S.F. Blake, E.J. Li, T.A. Hallam, D.G. Chilton, W.K. Gourley, L.H. Boise, C.B. Thompson, and E.B. Thompson. 1997. Elevated expression of Bcl-2 and Bcl-x by intestinal intraepithelial lymphocytes: resistance to apoptosis by glucocorticoids and irradiation. *Int. Immunol*. 9:945–953. http://dx.doi.org/10.1093/intimm/9.7.945

Vantourout, P., and A. Hayday. 2013. Six-of-the-best: unique contributions of γδ T cells to immunology. *Nat. Rev. Immunol*. 13:88–100. http://dx.doi.org/10.1038/nri3384

Wagner, N., J. Löhler, E.J. Kunkel, K. Ley, E. Leung, G. Krissansen, K. Rajewsky, and W. Müller. 1996. Critical role for β7 integrins in formation of the gut-associated lymphoid tissue. *Nature*. 382:366–370. http://dx.doi.org/10.1038/382366a0

Wurbel, M.A., M. Malissen, D. Guy-Grand, E. Meffre, M.C. Nussenzweig, M. Richelme, A. Carrier, and B. Malissen. 2001. Mice lacking the CCR9 CC-chemokine receptor show a mild impairment of early T- and B-cell development and a reduction in T-cell receptor gammadelta(+) gut intraepithelial lymphocytes. *Blood*. 98:2626–2632. http://dx.doi.org/10.1182/blood.V98.9.2626

Wurbel, M.A., M. Malissen, D. Guy-Grand, B. Malissen, and J.J. Campbell. 2007. Impaired accumulation of antigen-specific CD8 lymphocytes in chemokine CCL25-deficient intestinal epithelium and lamina propria. *J. Immunol*. 178:7598–7606.

Yu, W., Z. Misulovin, H. Suh, R.R. Hardy, M. Jankovic, N. Yannoutsos, and M.C. Nussenzweig. 1999. Coordinate regulation of RAG1 and RAG2 by cell type-specific DNA elements 5′ of RAG2. *Science*. 285:1080–1084. http://dx.doi.org/10.1126/science.285.5430.1080

Zabel, B.A., W.W. Agace, J.J. Campbell, H.M. Heath, D. Parent, A.I. Roberts, E.C. Ebert, N. Kassam, S. Qin, M. Zovko, et al. 1999. Human G protein-coupled receptor GPR-9-6/CC chemokine receptor 9 is selectively expressed on intestinal homing T lymphocytes, mucosal lymphocytes, and thymocytes and is required for thymus-expressed chemokine-mediated chemotaxis. *J. Exp. Med*. 190:1241–1256. http://dx.doi.org/10.1084/jem.190.9.1241

Zatz, M.M., and E.M. Lance. 1970. The distribution of chromium 51-labelled lymphoid cells in the mouse. A survey of anatomical compartments. *Cell. Immunol*. 1:3–17. http://dx.doi.org/10.1016/0008-8749(70)90057-2